




## Article

# Multi-UAV Coverage through Two-Step Auction in Dynamic Environments

Yihao Sun <sup>†</sup> , Qin Tan <sup>†</sup>, Chao Yan , Yuan Chang , Xiaojia Xiang and Han Zhou <sup>\*</sup>

College of Intelligence Science and Technology, National University of Defense Technology, Changsha 410073, China; sunyihao@nudt.edu.cn (Y.S.); tanqin20@nudt.edu.cn (Q.T.); yanchao17@nudt.edu.cn (C.Y.); changyuan10@nudt.edu.cn (Y.C.); xiangxiaojia@nudt.edu.cn (X.X.)

<sup>\*</sup> Correspondence: zhouhan@nudt.edu.cn

<sup>†</sup> These authors contributed equally to this work.

**Abstract:** The cooperation of multiple unmanned aerial vehicles (Multi-UAV) can effectively solve the area coverage problem. However, developing an online multi-UAV coverage approach remains a challenge due to energy constraints and environmental dynamics. In this paper, we design a comprehensive framework for area coverage with multiple energy-limited UAVs in dynamic environments, which we call MCTA (Multi-UAV Coverage through Two-step Auction). Specifically, the online *two-step auction* mechanism is proposed to select the optimal action. Then, an obstacle avoidance mechanism is designed by defining several heuristic rules. After that, considering energy constraints, we develop the *reverse auction* mechanism to balance workload between multiple UAVs. Comprehensive experiments demonstrate that MCTA can achieve a high coverage rate while ensuring a low repeated coverage rate and average step deviation in most circumstances.

**Keywords:** multi-UAV; two-step auction; area coverage; obstacle avoidance; energy constraint



**Citation:** Sun, Y.; Tan, Q.; Yan, C.; Chang, Y.; Xiang, X.; Zhou, H. Multi-UAV Coverage through Two-Step Auction in Dynamic Environments. *Drones* **2022**, *6*, 153. <https://doi.org/10.3390/drones6060153>

Academic Editor: Abdessattar Abdelkefi

Received: 30 May 2022

Accepted: 17 June 2022

Published: 20 June 2022

**Publisher's Note:** MDPI stays neutral with regard to jurisdictional claims in published maps and institutional affiliations.



**Copyright:** © 2022 by the authors. Licensee MDPI, Basel, Switzerland. This article is an open access article distributed under the terms and conditions of the Creative Commons Attribution (CC BY) license (<https://creativecommons.org/licenses/by/4.0/>).

## 1. Introduction

Unmanned aerial vehicles (UAV) have the characteristics of low operating cost, good maneuverability, and no risk of casualties [1,2]. Accordingly, it has been applied to many fields, such as surveying and mapping [3], surveillance [4], bathymetry [5–9], and disaster rescue [10,11]. As a typical application, area coverage with UAVs has attracted great attention in robotics. Its main objective is to move single UAV or a group of UAVs to cover a given area [12]. Compared with single UAV, area coverage with multiple UAVs has significant advantages. First, due to the workload distribution and collaboration, multi-UAV can efficiently complete the task. Second, it enhances robustness against component failure due to redundancy. Therefore, multiple cooperative UAVs are expected to play an important role in the area coverage field.

Although considerable efforts have been devoted to addressing the area coverage problem for multi-UAV, there are still some challenges that need to be resolved. For instance, most of the existing studies assume that different obstacles are equal and insurmountable [13]. However, the real environment may contain obstacles with different threat levels. In addition, existing studies do not consider energy constraints, and their effectiveness is only verified in simple scenarios. Furthermore, some studies ignore the interaction among multiple UAVs, which may lead to conflicts between UAVs [14].

In light of this, we further investigate multi-UAV for cooperative area coverage. Compared with the previous work, we take the energy constraint and workload balance of multi-UAV into consideration and solve a more challenging coverage problem.

### 1.1. Related Work

In the field of robotics, much work has been done to solve the area coverage problem. Khamis et al. [15] proposed an auction algorithm for multi-robot systems. Xin et al. [13]

proposed an auction-based spanning-tree coverage algorithm, which ensures the connectivity of each spanning tree and tries to balance the workload between robots. However, the above algorithms are difficult to achieve online planning of area coverage actions due to the lack of global information.

To address the limitation above, Viet et al. [14] proposed an online method based on boustrophedon motions. After reaching the critical point, the intelligent backtracking mechanism based on the suggested A\* search was applied to reach the starting point with the shortest collision-free path. Khan et al. [16] used a reputation-based auction mechanism to model the interaction between the UAV operators serving in close-by areas, achieving a strategic balance of control. It should be noted that the environment they considered was too simplistic, making their algorithm unable to adapt to the naturally dynamic environment.

In addition, the setting of dynamic obstacles is also crucial to adapt to the real environment in the field of area coverage. Gabriely and Rimon [17] proposed a spanning tree coverage algorithm based on a grid network. Sonti et al. [18] extended the set of path planning in an environment with static obstacles. Gorbenko et al. [19] studied an effective algorithm for multi-robot forest coverage underweighted terrain, which is suitable for solving synthetic terrain with real-world weight and special hard terrain. Roi Yehoshua et al. [20] divided the obstacles' threat to UAVs into five levels. They proposed a spanning tree-based coverage algorithm to meet the complexity of the real environment and the decision makers requirements for different targets. Nevertheless, most of these studies ignore the influence of energy constraints.

At the same time, the introduction of energy constraints is suitable for practical application scenarios [21–25]. Strimel et al. [26] introduced a new full-coverage planning algorithm that considers the robot's fixed fuel or energy capacity. Dutta et al. [27] proposed a constant-factor approximation algorithm for real-time coverage path planning with energy constraints. They studied the coverage planning problem of mobile robots with a limited energy budget, aimed to minimize the total travel distance covered by the environment and the number of visits to the charging station. However, covering as many low-risk areas as possible under energy constraints is still a challenge.

### 1.2. Contributions

In this paper, we presents a novel online planning solution of area coverage for multi-UAV in dynamic environments. The main contributions of this paper are as follows:

- We design the comprehensive MCTA framework for area coverage with multiple energy-limited UAVs in dynamic environments.
- We propose the two-step auction mechanism to select the optimal next action and avoid dynamic obstacles.
- We develop a reverse auction mechanism to avoid conflicts and balance workloads between UAVs.

The remainder of this paper is organized as follows: Section 2 formulates the area coverage problem. Section 3 presents our MCTA framework. In Section 4, a series of experiments are conducted to evaluate the performance of MCTA. Finally, Section 5 concludes the major findings and outlines the potential direction for future work.

## 2. Problem Formulation

As illustrated in the left of Figure 1, we employ  $v$  energy-limited UAVs to simultaneously cover a given square area with potential threats. The square area is rasterized into  $m^2$  basic square *units* with side length  $D$  (Figure 2). Each unit has a threat level  $\eta \in [0, 1]$ . The unit with  $\eta = 0$  means a safe unit, and the UAV can pass freely. The unit with  $0 < \eta < 1$  means there is a potential threat to UAVs, but the UAV can still pass. The unit with  $\eta = 1$  means an extremely dangerous obstacle which the UAV cannot pass. We assume that each UAV can only acquire the threat level of the units within its *sensing scope*, and it can move in four base directions, i.e., up, down, left, and right. As shown in Figure 2, we define a

*module* as a square composed of four units and treat the center point of the module as an equivalent replacement. Then, we define the modules that the UAV can reach in one time step as the *auction scope*.

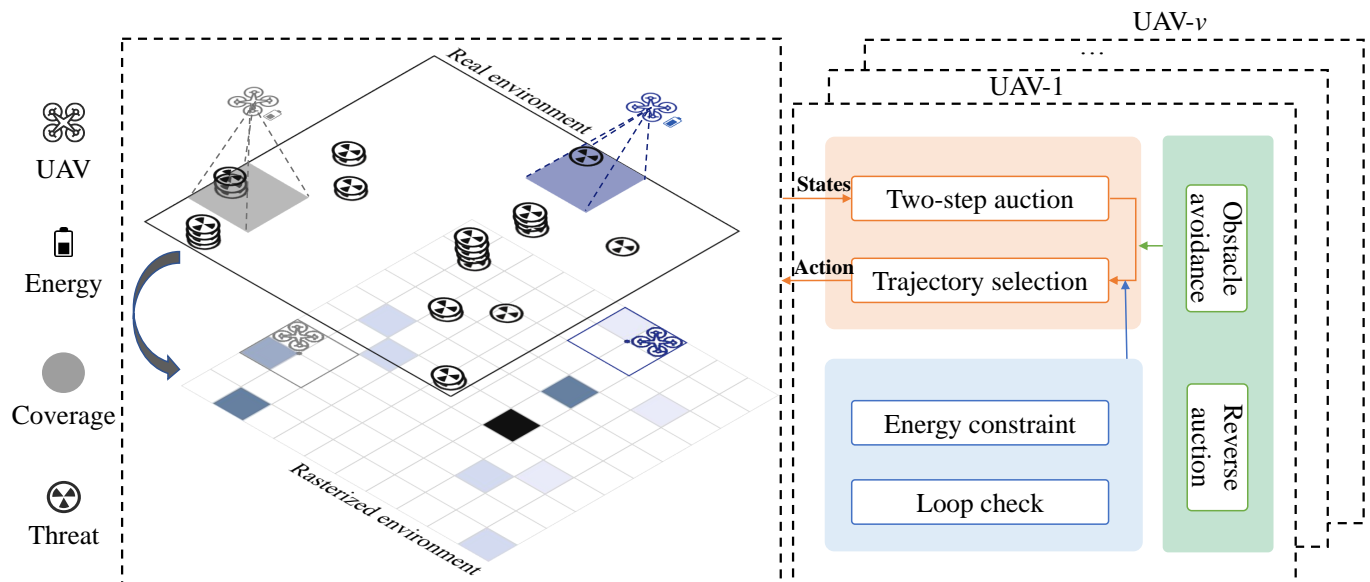


**Figure 1.** The proposed MCTA framework. The scenario on the left depicts the multi-UAV coverage process. The blocks on the right list key modules of MCTA.

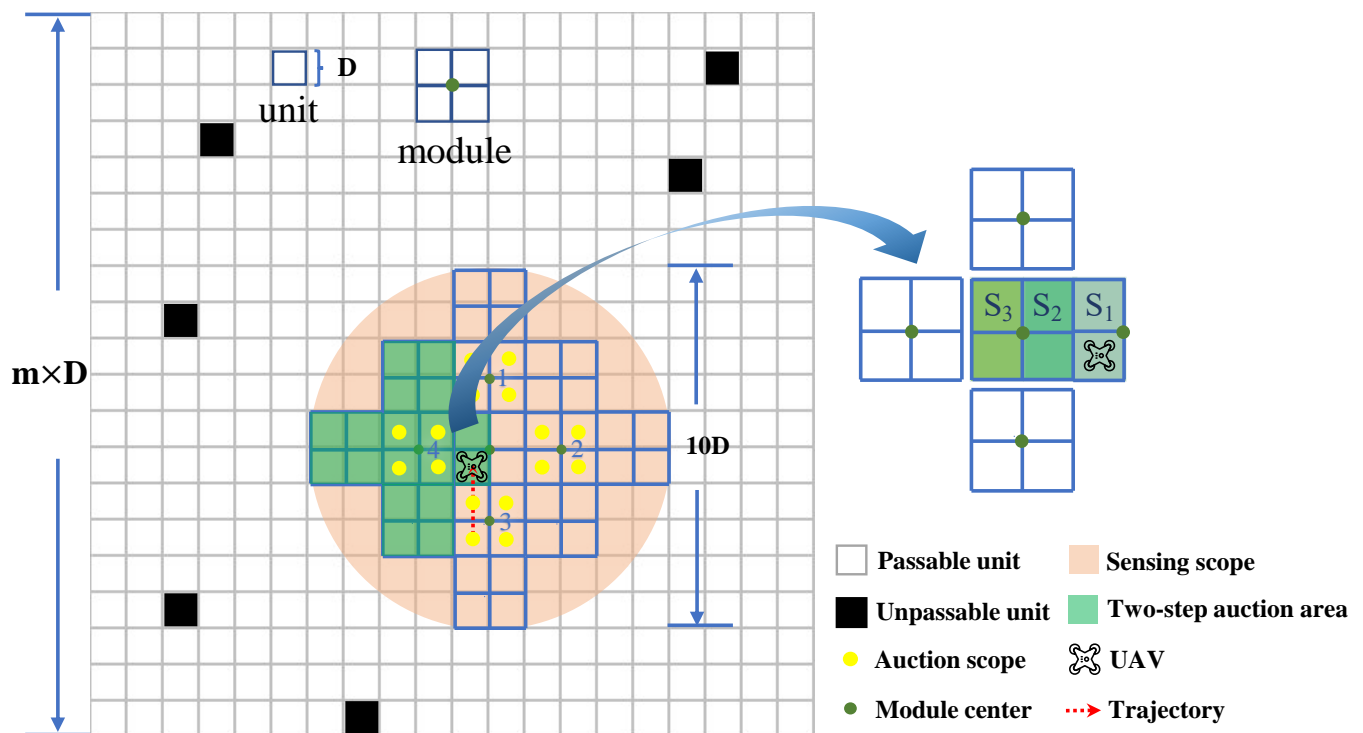


**Figure 2.** A square area is rasterized into  $m^2$  basic square units with side length  $D$ . A module is composed of four basic units.

Let a set of continuous units  $\{f_{i,k,1}, f_{i,k,2}, \dots\}$  denote the trajectory  $F_{i,k}$  of UAV<sub>*i*</sub> ( $i = 1, 2, \dots, v$ ) in the  $k$ th step, where  $f_{i,k,p}$  is the  $p$ th in the  $k$ th time step of UAV<sub>*i*</sub>'s position on the sequence. Denote the flight mileage (i.e., the number of accumulated passed units)

of UAV<sub>*i*</sub> in time step *k* as  $l_{i,k}$ . The total flight mileage  $L_i$  of UAV<sub>*i*</sub> at the end of the coverage task can be defined as:

$$L_i = \sum_k l_{i,k}. \quad (1)$$

In the coverage process, the remaining energy  $B_{i,k}$  of UAV<sub>*i*</sub> in the *k*th time step is related to its current flight mileage  $\sum_{k=0}^k l_{i,k}$ . The initial energy of each UAV is set as  $B$ , i.e.,  $B_{i,0} = B$ . Introducing different initial energy to the problem is sure to be more challenging, but in this paper, we only consider the case where each individual is equivalent to better analyze the completion of the coverage task. The UAV has two modes: work mode and sleep mode. In the process of coverage, the UAV is in work mode. In sleep mode, UAV will not perform the coverage task.

Our goal is to develop an online planning strategy of area coverage that enables multiple energy-limited UAVs to cover as many passable units as possible while avoiding collisions with other UAVs and obstacles. In other words, we expect to complete this coverage task with a higher coverage rate  $C_r$ , lower repetitive coverage rate  $R_r$ , and lower average flight deviation  $AD$ . The optimization objective is defined as:

$$\min \quad [-C_r, R_r, AD], \quad (2a)$$

$$\text{s.t.} \quad \forall i \in \{1, 2, \dots, v\}, L_i \leq B, \quad (2b)$$

$$\forall i, j \in \{1, 2, \dots, v\}, i \neq j, f_{i,k,p} \cap f_{j,k,p} = \emptyset, \quad (2c)$$

where constraint (2b) means the UAV cannot continue searching after its energy is exhausted. Constraint (2c) means no collision between UAVs.

### 3. MCTA Framework

In this section, we introduce the multi-UAV coverage through two-step auction framework. We first elaborate the two-step auction algorithm, which gives the bidding result of four adjacent modules to the UAV. Then, we focus on obstacle avoidance and multi-UAV conflict resolution. The UAV may take those strategies when the auction process ends. After that, we introduce the energy constraint model and loop-check mechanism. Finally, by assembling those modules above, we develop our framework. The details of each process are described in the following subsections.

#### 3.1. Two-Step Auction

In the online environment, the UAV only knows the local information within its exploration scope. To achieve the optimal coverage result with the limited information, we design the two-step auction algorithm (Algorithm 1).

To distinguish the effect of obstacles in different positions, we divide the auction scope of the UAV into three areas and set different weights  $W_d$  ( $d = 1, 2, 3$ ) for areas  $S_1$ ,  $S_2$ , and  $S_3$ . As shown in Figure 2, area  $S_1$  is a set of units in the current module that are close to the adjacent module. Area  $S_2$  is a set of basic units in adjacent modules that are closest to the module center where the UAV is located. Similarly, area  $S_3$  is a set of basic units in adjacent modules that are far away from the module center where the UAV is located. Considering that the obstacles which are extremely close or far away from the UAV have relatively little influence on covering the neighbor module, we set  $W_2 > W_1 > W_3$ .

In order to reduce the risk during the coverage process, the UAV will evaluate the threat level  $\zeta$  of the module to determine the future flight trajectory [20].  $\zeta$  is given as follows:

$$\zeta = \sum (\eta W_d), \quad (3)$$

where  $\eta$  is the threat level of the unit. The UAV will give priority to covering modules with lower  $\zeta$  and then cover modules with higher  $\zeta$  to reduce risks.

To make the UAV “see” farther, we design the two-step auction mechanism. In this mechanism, module centers in the auction scope bid to the UAV according to the

distribution of obstacles in the corresponding two-step auction area. The auction result of four modules can be written as set  $C = \{c_1, c_2, c_3, c_4\}$ . Here, we define the bid value  $c_i$  of module  $m_i$  as:

$$c_i = \frac{1}{\zeta_i + \zeta_m}. \quad (4)$$

The bid value  $c_i$  consists of two parts. First, we calculate  $\zeta_i$  of module  $m_i$  according to Equation (3). Then, we assume that the UAV is in module  $m_i$ , then calculate the  $\zeta$  of module  $m_1$ ,  $m_2$ , and  $m_4$  corresponding to module  $m_i$  and record the maximum value as  $\zeta_m$ . To make the UAV preferentially cover modules with lower threat levels, the bidding value of modules should be negatively related to their threat levels. When the bidding price of adjacent module centers is the same, the energy loss will be considered: the greater the turning angle, the greater the energy loss [28]. To reduce the negative effect of turning, we set the module priority level  $m_1 > m_2 > m_4 > m_3$ .

After obtaining the auction result from all adjacent modules, the UAV will determine the *winning module*, that is, the module corresponding to  $m'_1$  (Algorithm 1, line 7). Then, the UAV plans to reach the winning module. In other words, the two-step auction algorithm informs the desired position for the UAV.

---

**Algorithm 1** Two-step Auction.

---

**Input:** UAV position  $p$ , orientation  $o$

**Output:** Four models sorted by bidding price  $c_i$  and orientation  $o$

---

```

1: for  $i \leftarrow 1$  to 4 do
2:    $c_i \leftarrow \zeta_i$ ;
3:   Assume that the UAV is in module  $m_i$ ;
4:   Based on module  $m_i$ , calculate  $\zeta_m = \max(\zeta_1, \zeta_2, \zeta_4)$ ;
5:    $c_i \leftarrow \frac{1}{c_i + \zeta_m}$ ;
6: end for
7:  $\{m'_1, m'_2, m'_3, m'_4\} \leftarrow \text{sort}(\{c_1, c_2, c_3, c_4\}, o)$ ;
8: return  $\{m'_1, m'_2, m'_3, m'_4\}$ 

```

---

### 3.2. Obstacle Avoidance and Multi-UAV Conflict Resolution

After determining the winning module that it plans to arrive at, the UAV may not actually reach the module due to obstacles or multi-UAV conflicts. Even if a module is accessible, the UAV also has to choose a suitable way to reach it. Therefore, the avoidance of obstacles and the resolution of multi-UAV conflicts should be taken into consideration.

First, we introduce the obstacle avoidance strategy. Assume that the UAV is not able to overcome an obstacle by going over it. As shown in Figure 3, we give the specific path selection method based on obstacles in different locations. When the UAV cannot enter the next module, it does not fly to the corresponding module center. At this time, the UAV will re-select the second-best module in the current auction bidding process. If the UAV can access none of the four module centers involved in the bidding, it enters sleep mode and stops covering.

Then, we develop a conflict resolution strategy to solve this situation in that two or more UAVs bid a certain module at the same time. The key insight behind this strategy is the conflicting module center selects the UAV reversely, which can be regarded as a reverse auction. When the conflict occurs, the module will give priority to choosing the UAV that has encountered “unfair” treatment: the one that has the least flight mileage  $L$ . After the UAV is selected, other UAVs will pause for one time step and wait for the winning UAV to pass. Finally, all UAVs continue to execute the two-step auction process, select the module plan to reach, and continue the covering process.

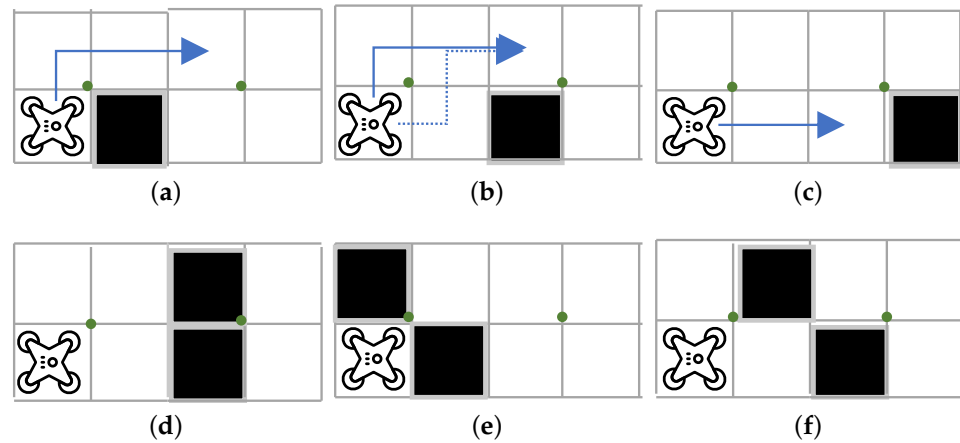


**Figure 3.** Six obstacle distributions and the UAV's corresponding path selection method. (a) The obstacle is located in area  $S_1$ . The UAV will turn into the next module. (b) The obstacle is located in area  $S_2$ . The UAV turns into the next module. (c) The obstacle is located in area  $S_3$ . The UAV goes straight into the next module. (d) Double obstacles located in area  $S_2$ . The UAV cannot enter the next module. (e) The obstacle is located in the neighbor unit of the unit where the UAV of the current module is located. The UAV cannot fly to the next module. (f) The obstacle is located in the neighbor unit in the direction of the winning module and the opposite unit in the current module. The UAV cannot fly to the next module.

### 3.3. Energy Constraint and Loop-Check

In addition to a higher coverage rate, the framework also has requirements for reducing the repetitive coverage rate and the average flight deviation. If the UAV cannot enter the sleep mode at an appropriate time, the convergence of the framework cannot be guaranteed, and it will also cause a higher repetitive coverage rate and average flight deviation. Based on this, we proposed the energy constraint model and the loop-check mechanism.

In the energy constraint model, the energy of the UAV<sub>*i*</sub> decays as the flight mileage  $L_i$  increases. The remaining energy  $B_{i,k}$  of UAV<sub>*i*</sub> in the  $k$ th time step is defined as:

$$B_{i,k} = B - \sum_{k=0}^k l_{i,k}, \quad (5)$$

where  $B$  is the initial energy of the UAV, that is, the UAV is allowed to travel at most  $B$  units.

Moreover, if the UAV's surrounding obstacles are distributed similarly during the flight process, it may fly back and forth. We define the trajectory generated by the back and forth flying as a loop. This loop increases the repeated coverage rate and leads to energy waste. To avoid the two negative effects, the UAV should do a loop-check. If the UAV enters the loop, it will enter into sleep mode.

In summary, for UAV<sub>*i*</sub>, if its remaining energy  $B_{i,k} = 0$ , or it is judged to enter the loop, or there are no passable modules, it will enter into sleep mode. That is, the UAV no longer participates in the auction process and stops covering. This theoretically guarantees that our framework will converge.

### 3.4. MCTA Framework

Combining those mechanisms above, each UAV cooperates to complete the coverage task in a complex dynamic environment (Algorithm 2). During the multi-UAV coverage process, if all UAVs enter into sleep mode, the whole coverage will end. It is worth mentioning that our framework is also suitable for the single-UAV or fixed obstacle situation, which is a degraded version of solving multi-UAV and dynamic environment problems. In



the following section, we will conduct related experiments to evaluate the performance of our framework.

---

**Algorithm 2** MCTA.

---

**Input:**  $p_i[k]$ ,  $orientation_i[k]$ ,  $plan\_poses$ ,  $i = 1, 2, \dots, v$

```

1:  $\{m'_1, m'_2, m'_3, m'_4\} \leftarrow \text{Two-step Auction}(p_i[k], o_i[k]);$ 
2:  $plan\_flag_i \leftarrow 0;$ 
3: for  $j \leftarrow 1$  to 4 do
4:   if module  $m$  corresponding to  $m'_j$  is reachable then
5:      $orientation_i[k+1] \leftarrow \text{direction of module } m;$ 
6:      $plan\_flag_i \leftarrow 1;$ 
7:     break
8:   end if
9: end for
10: if  $plan\_flag_i = 1$  then
11:   Judge if there is a multi-UAV conflict;
12:   if no conflict occurs or win the conflict then
13:     Check the remaining energy  $B_{i,k}$  and the loop;
14:     if  $B_{i,k} > 0$  and not in the loop then
15:       Choose a suitable way to reach module  $m$ ;
16:        $p_i[k+1] \leftarrow \text{the position of module } m;$ 
17:     else
18:        $mode_i \leftarrow \text{sleep};$ 
19:     end if
20:   else
21:     Stay in place for next step;
22:   end if
23: else
24:    $mode_i \leftarrow \text{sleep};$ 
25: end if
```

---

#### 4. Experiments and Analysis

This section demonstrates the performance of MCTA by conducting a series of experiments. We first show the effectiveness of MCTA in a typical environment with a single UAV and four UAVs. Then, the adaptability and the scalability are verified through the quantitative experiments with different UAV numbers and energy constraints.

##### 4.1. Qualitative Evaluation

We first evaluate the feasibility of MCTA for only one UAV. In the experiment, we set 10% obstacles in the given environment ( $N = 10\% \times M$ ) and allow obstacles to move randomly. We assume that obstacles of different  $\eta$  have different mobility capabilities: the higher the  $\eta$ , the smaller the obstacle's moving range. Specifically, the position of the obstacle is  $(x, y)$  before moving and changes to  $(x + m, y + m)$  after moving, where  $m$  is a random integer generated from the closed interval  $[-a, a]$ . The specific mapping relationship between  $\eta$  and  $a$  is given in Table 1.

**Table 1.** The mapping of  $\eta$  and  $a$ .

$\eta$	0.2	0.4	0.6	0.8	1
$a$	4	3	2	1	0 (obstacles cannot move)

Figure 4 shows the coverage process with single UAV under a  $20 \times 20$  dynamic environment. Different colors represent different  $\eta$  of obstacles: the darker the obstacle, the higher the threat level. Figure 4a illustrates the initial situation: obstacles with different  $\eta$

are distributed in different positions and the UAV is ready to perform its coverage mission. Figure 4b shows the coverage performance when the time step = 20. At this time, there are about 1/5 green units (units covered for the first time) and no brown units (units covered twice or more), which means that the UAV is actively exploring the new area. The coverage result is given in Figure 4c. Obviously, only few units are not covered.

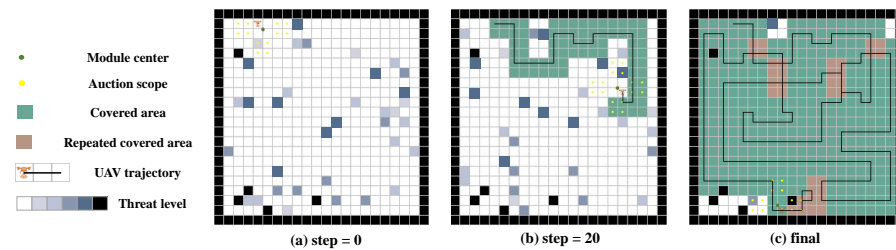


**Figure 4.** The evolution of coverage with a single UAV. The area covered for the first time is filled in green, and the area covered twice or more is filled in brown. After the UAV performs related flight actions, it will generate its own flight trajectory (the black line).

Then, we test the performance of MCTA with four UAVs in the same environment. In Figure 5a, the position of UAV<sub>2</sub> is (1, 2), and the position of UAV<sub>3</sub> is (1, 1); therefore, they may encounter a conflict in the next time step due to their adjacent positions. However, from the trajectories of two UAVs in Figure 5b, the conflict did not happen, which indicates our reverse auction mechanism works. In addition, compared with Figure 4b, Figure 5b has significantly more green units. It shows the advantages of multi-UAV coverage in terms of efficiency. In the final time step (Figure 5c), we extract and compare the length of each UAV<sub>i</sub>'s trajectory and find that they are almost the same (Figure 5d). This means the balanced workload between UAVs. Although the coverage rate of four UAVs is almost same with that of the single UAV, the whole coverage process of four UAVs ends faster. As a result, the coverage with multiple UAVs is more efficient.

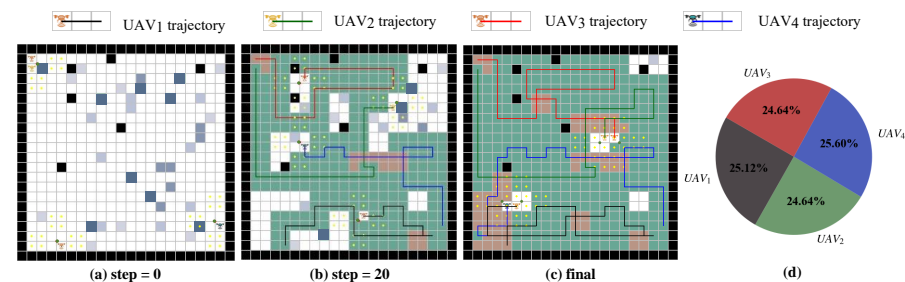


**Figure 5.** The evolution of coverage with four UAVs. Compared with single UAV, in a similar initial environment (a), multiple UAVs can achieve better coverage performance before the framework converges (b). In the final time step (c), different trajectories are shown in different colors. The pie chart (d) illustrates the proportion of each UAV's trajectory length.

In summary, the MCTA framework can obtain a high coverage rate regardless of single-UAV or multi-UAV situations. Moreover, it realizes the avoidance of conflicts and balances the workload between multiple UAVs. This indicates the adaptability and effectiveness of our framework in dynamic and complex environments.

#### 4.2. Quantitative Evaluation

In this subsection, we introduce the following metrics to further evaluate the quantitative performance of MCTA:

- **Coverage rate:** The coverage rate  $C_r$  is defined as the ratio between the area of covered modules and the area of the entire environment:

$$C_r = \frac{|F_1 \cup F_2 \cup \dots \cup F_v|}{M} \times 100\%, \quad (6)$$



where  $F_i$  is the set of  $F_{i,k}$ ,  $|\cdot|$  represents the number of elements in a set, and  $F_1 \cup F_2 \cup \dots \cup F_v$  represents the union of all UAV flight trajectories.

• **Repeated coverage rate:** The repeated coverage rate  $R_r$  is defined as:

$$R_r = \frac{\sum_{i,k} (l_{i,k} - |F_{i,k}|)}{|F_1 \cup F_2 \cup \dots \cup F_v|} \times 100\%, \quad (7)$$

where  $\sum_{i,k} (l_{i,k} - |F_{i,k}|)$  represents the difference between the flight mileage of all UAVs and the number of units passed by the flight trajectory, that is, the units that are repeatedly covered are accumulated by the frequency of coverage.

• **Average flight deviation:** To investigate the degree of deviation of the flight path of each UAV from its average path, the average flight deviation  $AD$  is defined as follows:

$$AD = \frac{1}{v} \sum_i \text{abs}(L_i - \bar{L}), \quad (8)$$

where  $\bar{L}$  is the average flight mileage.  $AD$  measures whether the workload of each UAV is balanced.

After that, we enrich the environments to challenge the adaptability of our framework quantitatively. As shown in Figure 6, *env-free* is the simplest environment. It is also the environment of the previous subsection; *env-strip* illustrates the staggered distribution of obstacles and its passable routes are less than *env-free*; In *env-convex*, we set a regular border, which brings a challenge to achieve complete coverage; on the basis of *env-convex*, we set up a non-convex *env-ring*. Its passable area is similar to the loop; in *env-honeycomb* and *env-maze*, the border becomes more complicated and both of them increase the risk of UAVs falling into loops.

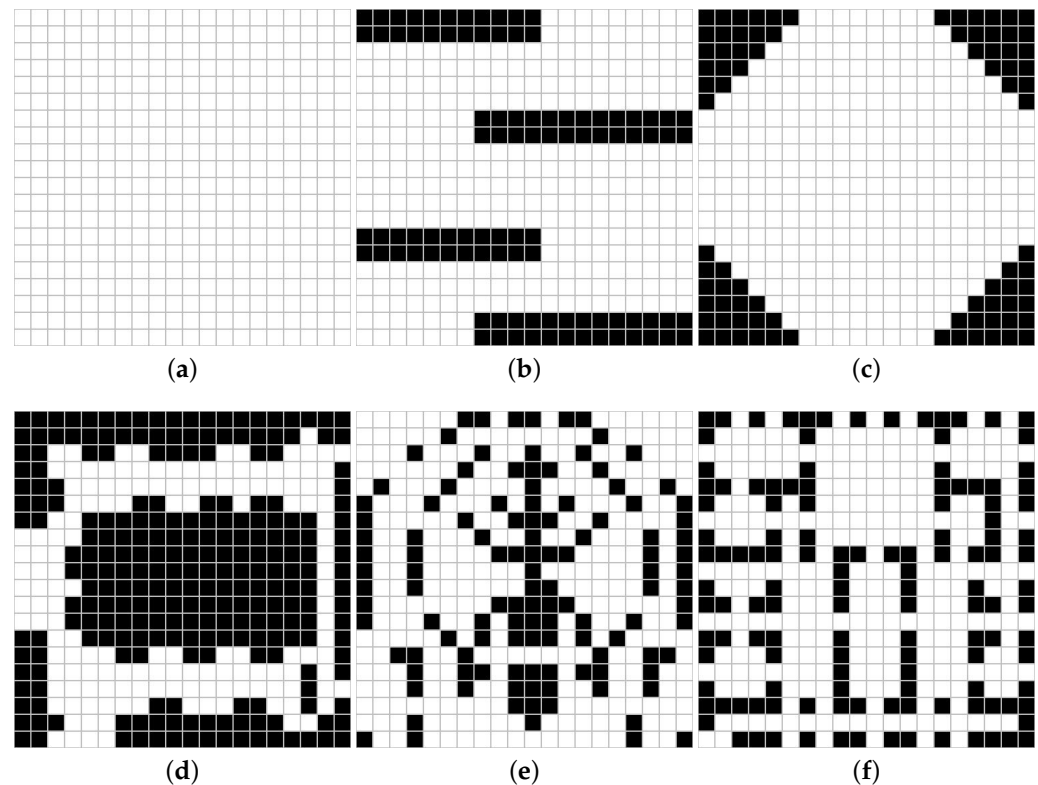


**Figure 6.** Configuration spaces of the (a) free, (b) strip, (c) convex, (d) ring, (e) honeycomb, and (f) maze.

Table 2 provides part of quantitative experimental results. In simple environments (i.e., *env-free*, *env-strip*, and *env-convex*), increasing the number  $v$  of UAVs will increase  $R_r$  but makes little contributions to  $C_r$ . In this case, if the convergence time is not considered, single UAV performs better than multiple UAVs. However, in complex environments (i.e., *env-ring*, *env-honeycomb*, and *env-maze*), increasing the number of UAVs can increase  $C_r$  obviously. At this time, multiple UAVs have more advantages. Then, we compared the  $C_r$ ,  $R_r$ , and  $AD$  in static and dynamic environments separately and found that they were almost the same. This shows that the MCTA framework can overcome the negative effects of uncertain factors caused by the dynamic environment. Moreover, most of  $C_r$  can reach more than 90%,  $R_r$  are generally less than 50%, and  $AD$  are about 3. Therefore, our framework can make the UAV complete coverage tasks efficiently in complex environments.

**Table 2.**  $C_r$ ,  $R_r$ , and  $AD$  of MCTA under different configurations.

Environment	Size	$v$	Static			Dynamic		
			$C_r$	$R_r$	$AD$	$C_r$	$R_r$	$AD$
free	$20 \times 20$	1	93.54%	15.66%	0	93.06%	14.87%	0
		4	92.18%	23.37%	1.34	91.98%	23.32%	1.44
		8	88.14%	25.11%	1.41	88.52%	24.66%	1.44
	$40 \times 40$	1	91.06%	19.30%	0	91.74%	19.75%	0
		4	91.09%	23.39%	2.26	91.08%	23.92%	2.41
convex	$20 \times 20$	1	96.34%	30.32%	0	96.52%	31.40%	0
		4	95.59%	38.91%	1.58	96.28%	40.17%	1.6
		12	92.42%	49.06%	1.4	92.70%	48.36%	1.36
	$40 \times 40$	1	94.58%	33.51%	0	94.73%	32.47%	0
		8	95.39%	43.23%	3.9	95.40%	43.24%	3.86
		12	95.08%	45.48%	2.74	95.20%	45.78%	2.74
maze	$20 \times 20$	8	81.89%	33.32%	3.42	80.53%	35.26%	3.4
		12	82.36%	38.42%	2.64	82.67%	41.01%	2.43
	$40 \times 40$	1	79.47%	29.80%	0	79.75%	29.97%	0
		12	87.07%	45.11%	9.13	87.67%	45.29%	8.93
ring	$20 \times 20$	1	83.02%	22.78%	0	83.44%	24.26%	0
		12	86.82%	46.64%	1.35	86.43%	47.05%	1.43
	$40 \times 40$	1	81.27%	33.76%	0	80.81%	32.32%	0
		12	89.09%	49.53%	2.95	88.42%	50.27%	2.97
honeycomb	$20 \times 20$	1	75.74%	36.19%	0	75.75%	35.62%	0
		8	80.75%	37.57%	3.27	80.45%	37.95%	3.33
strip	$20 \times 20$	1	92.07%	28.82%	0	93.15%	29.16%	0
		4	93.31%	39.58%	3.26	93.70%	39.52%	2.96
		8	93.30%	45.57%	1.82	92.89%	44.94%	1.85
	$40 \times 40$	1	87.42%	28.94%	0	87.86%	30.27%	0
		12	92.13%	46.28%	4.83	92.61%	45.93%	4.88

Of course, in individual environments, MCTA performs relatively poorly, such as  $20 \times 20$  *env-honeycomb* and  $40 \times 40$  *env-maze*. Regardless of the number  $v$ ,  $C_r$  is typically less than 90%, and  $R_r$  is also relatively high. This is probably caused by the complexity and disconnectivity of the environment, where UAVs are prone to fall into the local optimal solution.

Figure 7 shows the final  $C_r$ ,  $R_r$ , and  $AD$  of different  $v$  under different  $20 \times 20$  environments. In Figure 7a, when  $v$  changes from 4 to 8,  $C_r$  increases very obviously. However, when  $v$  changes from 8 to 12,  $C_r$  does not increase significantly, and sometimes even decreases. At the same time, we also noticed that in the three corresponding environments in Table 2,  $AD$  usually increases significantly when the number  $v$  increases sharply. We

attribute these two phenomena to frequent conflicts caused by excessive number of UAVs, which leads to the reduction of coverage efficiency. As a result, for the environment of a certain size, an appropriate increase in the number of UAVs can effectively improve the coverage rate, but an excessive number of UAVs may have a negative effect, because excess means diseconomy and poor coverage performance. Figure 7b,c show the  $R_r$  and  $AD$  of four UAVs under different initial energy in  $20 \times 20$  dynamic *env-free*. From the trend of the two histograms, it is clear that the larger initial energy of the UAV, the larger  $R_r$  and  $AD$ . This is exactly what we are expected on energy saving: to complete the coverage task, the UAV does not need too much initial energy.

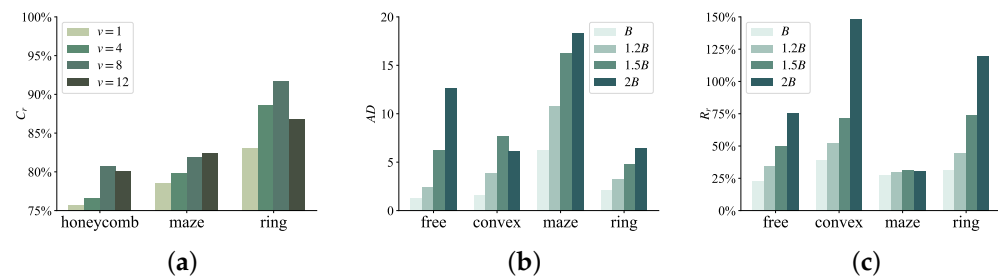


**Figure 7.** The performance of the MCTA framework under different configurations. (a) The coverage rate  $C_r$  under three complex environments (*env-honeycomb*, *env-maze*, and *env-ring*) in different numbers of UAVs (1, 4, 8, and 12). (b,c) The number  $v$  of UAVs is fixed to 4 and the average flight deviation  $AD$  and repeated coverage rate  $R_r$  are shown with different initial energy ( $B$ ,  $1.2B$ ,  $1.5B$ , and  $2B$ ) in two simple environments (*env-free* and *env-convex*) and two complex environments (*env-maze* and *env-ring*).

Considering all factors, to achieve a better search coverage result, for *env-freedom*, *env-convex*, and  $20 \times 20$  *env-strip*, the best number of UAVs is 1. For  $20 \times 20$  *env-maze* and *env-honeycomb*, the best number of UAVs is 8. Then, for  $40 \times 40$  *env-strip*, *env-maze*, and *env-ring*, the best number of UAVs is 12. In general, on the premise of achieving a high coverage rate, MCTA minimizes the repeated coverage rate and average step deviation as much as possible.

## 5. Conclusions

In this paper, we design an efficient framework for multiple UAVs in dynamic environments. The framework can be executed online and realizes the optimal solution within the exploration scope. A series of experiments have been conducted to demonstrate its superior coverage rate, scalability to the number of UAVs, and adaptivity to the dynamic environments. Note that the physical properties of the UAVs are not specified. The proposed multi-UAV collaborative coverage framework is generally applicable for systems with similar configurations.

In future work, we will take the non-linear change of the remaining battery into account, e.g., a UAV spends more energy to take off than other stages (such as hovering or moving sideways). Furthermore, another promising direction is to explore the upper bound number of UAVs. In addition, we would like to evaluate our framework through field experiments.

**Author Contributions:** Conceptualization, Y.S. and Q.T.; methodology, Q.T.; software, Y.S.; validation, Y.S. and Q.T.; formal analysis, Y.S., Q.T., C.Y. and Y.C.; investigation, Q.T.; writing—original draft preparation, Y.S. and Q.T.; writing—review and editing, C.Y. and Y.C.; supervision, X.X. and H.Z. All authors have read and agreed to the published version of the manuscript.

**Funding:** This research received no external funding.

**Institutional Review Board Statement:** Not applicable.

**Informed Consent Statement:** Not applicable.

**Data Availability Statement:** Not applicable.

**Acknowledgments:** The authors would like to thank the Swarm Observation and Regulation Laboratory, National University of Defense Technology, Hunan Province, China, for the resources provided by them.

**Conflicts of Interest:** The authors declare no conflict of interest.

## References

1. Liu, Z.; Wang, X.; Shen, L.; Zhao, S.; Cong, Y.; Li, J.; Yin, D.; Jia, S.; Xiang, X. Mission-oriented miniature fixed-wing UAV swarms: A multilayered and distributed architecture. *IEEE Trans. Syst. Man Cybern. Syst.* **2020**, *52*, 1588–1602. [\[CrossRef\]](#)
2. Yan, C.; Xiang, X.; Wang, C. Towards real-time path planning through deep reinforcement learning for a UAV in dynamic environments. *J. Intell. Robot. Syst.* **2020**, *98*, 297–309. [\[CrossRef\]](#)
3. Ball, Z.; Odonkor, P.; Chowdhury, S. A swarm-intelligence approach to oil spill mapping using unmanned aerial vehicles. In Proceedings of the AIAA Information Systems-AIAA Infotech@ Aerospace, Grapevine, TX, USA, 9–13 January 2017; p. 1157.
4. Pannozzi, P.; Valavanis, K.P.; Rutherford, M.J.; Guglieri, G.; Scanavino, M.; Quagliotti, F. Urban monitoring of smart communities using UAS. In Proceedings of the 2019 International Conference on Unmanned Aircraft Systems (ICUAS), Atlanta, GA, USA, 11–14 June 2019; pp. 866–873.
5. Alevizos, E.; Oikonomou, D.; Argyriou, A.V.; Alexakis, D.D. Fusion of Drone-Based RGB and Multi-Spectral Imagery for Shallow Water Bathymetry Inversion. *Remote Sens.* **2022**, *14*, 1127. [\[CrossRef\]](#)
6. Bandini, F.; Lopez-Tamayo, A.; Merediz-Alonso, G.; Olesen, D.; Jakobsen, J.; Wang, S.; Garcia, M.; Bauer-Gottwein, P. Unmanned aerial vehicle observations of water surface elevation and bathymetry in the cenotes and lagoons of the Yucatan Peninsula, Mexico. *Hydrogeol. J.* **2018**, *26*, 2213–2228. [\[CrossRef\]](#)
7. Specht, M.; Stateczny, A.; Specht, C.; Widźgowski, S.; Lewicka, O.; Wiśniewska, M. Concept of an Innovative Autonomous Unmanned System for Bathymetric Monitoring of Shallow Waterbodies (INNOBAT System). *Energies* **2021**, *14*, 5370. [\[CrossRef\]](#)
8. Stateczny, A.; Specht, C.; Specht, M.; Brčić, D.; Jugović, A.; Widźgowski, S.; Wiśniewska, M.; Lewicka, O. Study on the Positioning Accuracy of GNSS/INS Systems Supported by DGPS and RTK Receivers for Hydrographic Surveys. *Energies* **2021**, *14*, 7413. [\[CrossRef\]](#)
9. Wang, D.; Xing, S.; He, Y.; Yu, J.; Xu, Q.; Li, P. Evaluation of a New Lightweight UAV-Borne Topo-Bathymetric LiDAR for Shallow Water Bathymetry and Object Detection. *Sensors* **2022**, *22*, 1379. [\[CrossRef\]](#) [\[PubMed\]](#)
10. Lin, L.; Goodrich, M.A. UAV intelligent path planning for wilderness search and rescue. In Proceedings of the 2009 IEEE/RSJ International Conference on Intelligent Robots and Systems, St. Louis, MO, USA, 10–15 October 2009; pp. 709–714.
11. Kohlbrecher, S.; Kunz, F.; Koert, D.; Rose, C.; Manns, P.; Daun, K.; Schubert, J.; Stumpf, A.; von Stryk, O. Towards highly reliable autonomy for urban search and rescue robots. In *Proceedings of the Robot Soccer World Cup*; Springer: Berlin/Heidelberg, Germany, 2014; pp. 118–129.
12. Galceran, E.; Carreras, M. A survey on coverage path planning for robotics. *Robot. Auton. Syst.* **2013**, *61*, 1258–1276. [\[CrossRef\]](#)
13. Gao, G.Q.; Xin, B. A-STC: Auction-based spanning tree coverage algorithm formation planning of cooperative robots. *Front. Inf. Technol. Electron. Eng.* **2019**, *20*, 18–31. [\[CrossRef\]](#)
14. Viet, H.H.; Dang, V.H.; Laskar, M.N.U.; Chung, T. BA\*: An online complete coverage algorithm for cleaning robots. *Appl. Intell.* **2013**, *39*, 217–235. [\[CrossRef\]](#)
15. Khamis, A.; Hussein, A.; Elmogy, A. Multi-robot task allocation: A review of the state-of-the-art. *Coop. Robot. Sens. Netw.* **2015**, *2015*, 31–51.
16. Khan, A.S.; Chen, G.; Rahulamathavan, Y.; Zheng, G.; Assadhan, B.; Lambbotharan, S. Trusted UAV Network Coverage Using Blockchain, Machine Learning, and Auction Mechanisms. *IEEE Access* **2020**, *8*, 118219–118234. [\[CrossRef\]](#)
17. Gabriely, Y.; Rimon, E. Spiral-STC: An on-line coverage algorithm of grid environments by a mobile robot. In Proceedings of the 2002 IEEE International Conference on Robotics and Automation (Cat. No. 02CH37292), Washington, DC, USA, 11–15 May 2002; Volume 1, pp. 954–960.
18. Sonti, S.; Virani, N.; Jha, D.K.; Mukherjee, K.; Ray, A. Language measure-theoretic path planning in the presence of dynamic obstacles. In Proceedings of the 2013 American Control Conference, Washington, DC, USA, 17–19 June 2013; pp. 5110–5115.
19. Gorbenko, A.; Popov, V. The multi-robot forest coverage for weighted terrain1. *J. Ambient. Intell. Smart Environ.* **2015**, *7*, 835–847. [\[CrossRef\]](#)
20. Yehoshua, R.; Agmon, N.; Kaminka, G.A. Robotic adversarial coverage of known environments. *Int. J. Robot. Res.* **2016**, *35*, 1419–1444. [\[CrossRef\]](#)
21. Shnaps, I.; Rimon, E. Online coverage of planar environments by a battery powered autonomous mobile robot. *IEEE Trans. Autom. Sci. Eng.* **2016**, *13*, 425–436. [\[CrossRef\]](#)
22. Wei, M.; Isler, V. Coverage path planning under the energy constraint. In Proceedings of the 2018 IEEE International Conference on Robotics and Automation (ICRA), Brisbane, Australia, 21–25 May 2018; pp. 368–373.
23. Wu, C.; Dai, C.; Gong, X.; Liu, Y.J.; Wang, J.; Gu, X.D.; Wang, C.C. Energy-efficient coverage path planning for general terrain surfaces. *IEEE Robot. Autom. Lett.* **2019**, *4*, 2584–2591. [\[CrossRef\]](#)

24. Modares, J.; Ghanei, F.; Mastronarde, N.; Dantu, K. Ub-anc planner: Energy efficient coverage path planning with multiple drones. In Proceedings of the 2017 IEEE International Conference on Robotics and Automation (ICRA), Singapore, 29 May–3 June 2017; pp. 6182–6189.
25. Jensen-Nau, K.R.; Hermans, T.; Leang, K.K. Near-Optimal Area-Coverage Path Planning of Energy-Constrained Aerial Robots with Application in Autonomous Environmental Monitoring. *IEEE Trans. Autom. Sci. Eng.* **2020**, *18*, 1453–1468. [[CrossRef](#)]
26. Strimel, G.P.; Veloso, M.M. Coverage planning with finite resources. In Proceedings of the 2014 IEEE/RSJ International Conference on Intelligent Robots and Systems, Chicago, IL, USA, 14–18 September 2014; pp. 2950–2956.
27. Dutta, A.; Sharma, G. A Constant-Factor Approximation Algorithm for Online Coverage Path Planning with Energy Constraint. *arXiv* **2019**, arXiv:1906.11750.
28. Torres, M.; Pelta, D.A.; Verdegay, J.L.; Torres, J.C. Coverage path planning with unmanned aerial vehicles for 3D terrain reconstruction. *Expert Syst. Appl.* **2016**, *55*, 441–451. [[CrossRef](#)]